Laser pulse heating of steel surfaces including impinging gas effect and variable properties

S.Z. Shuja, B.S. Yilbas and M.O. Budair
Mechanical Engineering Department King Fahd University of Petroleum & Minerals, Dhahran, Saudi Arabia

Received February 2000
Revised May 2000
Accepted May 2000

Keywords *Surfaces, Heat conduction, Steel*

Abstract *The gas assisted laser heating of engineering surfaces finds wide application in industry. Numerical simulation of the heating process may considerably reduce the cost spent on experimentation. In the present study, 2-dimensional axisymmetric flow and energy equations are solved numerically using a control volume approach for the case of a gas assisted laser heating of steel surfaces. Various turbulence models including standard k-ε, k-ε YAP, low Reynolds number k-ε and RSTM models are tested. The low Reynolds number k-ε model is selected to account for the turbulence. Variable properties of both solid and gas are taken into account during the simulation. Air is considered as an assisting gas impinging the workpiece surface coaxially with the laser beam. In order to validate the presently considered methodology, the study is extended to include comparison of present predictions with analytical solution for the case available in the literature. It is found that the assisting gas jet has some influence on the temperature profiles. This effect is minimum at the irradiated spot center and it amplifies considerably in the gas side. In addition, account for the variable properties results in lower surface temperatures as compared to the constant properties case.*

Nomenclature

a	= coeffieient of ϕ in equation (16)	p	= pressure
b	= Gaussian parameter	Re	= Reynolds no.
c_p	= variable specific heat (function of temperature)	R	= reflectivity
C_1, C_2, C_μ	= cofficient in the k-ε turbulence model	r	= distance in the radial direction
D	= jet diameter	S	= unsteady spatially varying laser heat source (equation 9)
f_1, f_2, f_μ	= coefficient in the low Reynolds no, k-ε model	S_ϕ	= source term for variable ϕ
G	= rate of generation of k	S_0	= constant in source term
h	= heat transfer coefficient	S_p	= coefficient of ϕ In the source term
I_0	= peak power intensity	t	= time
K	= variable thermal conductivity (function of temperature)	T	= temperature
		T_0	= initial temperature in equation (17)
		T_∞	= free-stream temperature
k	= turbulent kinetic energy	u^*	= friction velocity

International Journal of Numerical Methods for Heat & Fluid Flow, Vol. 12 No. 2, 2002, pp. 195–219.

DOI 10.1108/09615530210418339

U = arbitrary velocity
$\forall$ = volume
V = radial velocity
x = arbitrary direction
z_n = distance to the nearest wall
z = distance in the axial direction

Greek

α = thermal diffusivity
Γ = arbitrary diffusion coefficient
δ = absorption coefficient
ε = energy dissipation
λ = turbulence intensity
μ = variable dynamic viscosity (function of temperature for laminar)
μ_e = effective viscosity ($\mu_l+\mu_t$)
ν = variable kinematic viscosity (function of temperature for laminar)
ρ = density (function of temperature and pressure for gas)
σ = variable Prandtl no. (function of temperature)
τ = pulse length which is 1.08 ms
Φ = viscous dissipation
ϕ = arbitrary variable

Subscript

amb = ambient
i, *j* = arbitrary direction
jet = gas jet at inlet
l = laminar
p = a typical node in the computational grid
Turbulent
n, s, e, w, l, h = north, south, east, west, low or high node
w = wall

1. Introduction

Laser heating of engineering surfaces has become a wide research field in recent years. Laser assisted manufacturing processes have encouraged the development of several model calculations of both spatial and temporal temperature profiles in laser heated solids (Schultz *et al.*, 1993; Loze and Wright, 1997; Al-Nimr and Masoud, 1997). However, two features of laser machining of materials need to be identified. These include low and high intensity radiation processing. Low intensity radiation may be considered when the heating process is conduction limited while high intensity radiation may apply for the non-conduction heating process (Yilbas, 1997). The pulsed laser heating is fruitful in surface treatment of engineering metals to obtain improved surface properties, such as hardness, corrosion and wear resistance (Osawa *et al.*, 1995). In order to establish better understanding of the heating mechanism, laser induced temperature rise becomes an important research area, since it has an important role in the laser induced physical and chemical processes.

The modeling of conduction limited laser heating in solids was previously investigated by several researchers, but only few compare the predictions with experimental findings (Sun *et al.*, 1996; Yilbas, 1993, and Qiu and Tien, 1994). Heating of a solid surface by a high power laser was carried out by Diniz Nero and Lima (1994). They considered variable properties of the workpiece and solved the three-dimensional nonlinear parabolic differential form of the diffusion equation while omitting the impinging gas jet effect. A numerical scheme was introduced in solving the governing equations, however, the grid

independent test was not discussed. Heat diffusion in the deep penetration welding was investigated by Simon *et al.* (1993). They predicted the temporal behavior of the surface temperature due to time-modulated laser beam pulses. They showed that the modulated beam had little effect on the resulting heat affected zone.

In the laser heat treatment process, an assisting gas is usually used to shield the surface of the non-metallic material treated from the high temperature oxidation reactions. When modeling such laser heating processes, the impinging gas jet needs to be considered. This involves a stagnation point flow for the case when the assisting gas impinges orthogonal to the heated surface. Therefore, investigation into stagnation point flow characteristics becomes important when modeling the laser gas assisted heating. The stagnation point flow has been investigated by several researchers (Yeckel *et al.*, 1994; Ariel, 1993, and Kerr and Dold, 1994), with some dealing with the heat transfer. A comprehensive review of semi-analytical solutions for flame impingement heat transfer was carried out by Baukal and Gebhart (1996). An alternative formulation for the freestream matching condition for stagnation point turbulent flows was introduced by Abid and Speziale (1996). The applicability of the standard k-e model in stagnation point flow was discussed. They argued that the e-transport equation was unable to predict the "production equals dissipation" hypothesis in conjunction with a free stream mean velocity field that corresponded to the homogeneous plane strain of turbulent flow. However, they introduced vortex stretching effects in the turbulent dissipation rate equation. Impinging jet studies for the turbulence model assessment were carried out by Craft *et al.* (1993). They indicated that the k-ε model and one of the Reynolds stress models predicted very high levels of turbulence near the stagnation point. The excessive energy predicted in turn induced too high heat transfer coefficients and turbulent mixing with the ambient fluid. An extension of the Lam Bremhorst two-equation turbulence model to variable density flows was described by Strahle *et al.* (1987), for two-dimensional plane stagnation-point flow. They developed a transport equation for temperature (density) fluctuations and indicated that the results predicted agreed well with the heat transfer data available at low Reynolds numbers. In light of the above arguments, the applicability of the turbulence models may highly depend on the flow and boundary conditions. The gas jet impingement during laser pulsative heating process was investigated previously for two gas jet velocities (Shuja and Yilbas, 1998).

The influence of gas velocity on the conjugate heating was not explored explicitly. Consequently, this effect needs to be examined in detail.

The present study is conducted to model the transient process of gas assisted laser heating of steel. An air jet is used as the assisting gas impinging onto the workpiece surface coaxial with the laser beam. Transient two-dimensional axisymmetric heating model with variable fluid and solid

properties is considered. The continuity, momentum, energy and equation of state are solved numerically using the control volume approach, for the conjugate heating process. To simulate the flow field various turbulence models are tested for stagnation flow due to jet impingement on an axisymmetric plane wall with a constant heat flux emanating over a limited area of the wall. These turbulence models include two variations of Reynolds stress model (Launder, 1989a; Launder, 1989b), high Reynolds number k-ε model with YAP correction and low Reynolds number k-ε model. Moreover, the predictions due to different turbulence models are compared with the previous experimental findings (Ashforth-Frost and Jambunathan, 1996). Consequently, based on the findings, low Reynolds number k-ε model gives acceptable results within reasonable computational time and is therefore selected to account for the turbulence. Since the gas jet velocity considered varies within the range of 1–300 m/s, a compressibility effect is taken into account for high gas jet velocities.

2. Formulation of the flow and energy equations

The fluid flow is assumed to reach a steady state before the laser heat source is switched on. Consequently, in order to obtain the initial conditions for laser heating the governing conservation equations are solved. Once the heat source is switched on the transient conservation equations in the gas side and the unsteady conduction equation the solid are solved. To simulate the actual process, a compressible flow with variable properties is considered while temperature dependent thermal conductivity and specific heat are taken into account for the solid substance.

2.1 Flow equations

To simulate the flow field due to jet impingement, two-dimensional axisymmetric form of the continuity and the time-averaged Navier-Stokes equations are considered. In the Cartesian Tensor system the continuity and momentum equations can be written in the following form:

$$\frac{\partial \rho}{\partial t} + \frac{\partial}{\partial x_i}(\rho U_i) = 0 \tag{1}$$

and

$$\frac{\partial}{\partial t}(\rho U_j) + \frac{\partial}{\partial x_i}(\rho U_i U_j) = -\frac{\partial p}{\partial x_j} + \frac{\partial}{\partial x_i}\left[(\mu_t + \mu_l)\frac{\partial U_j}{\partial x_i}\right] \tag{2}$$

The eddy viscosity μ_t, has to be specified by a turbulence model. Using the same analogy, the partial differential equation governing the transport of energy has the form:

$$\frac{\partial}{\partial t}(\rho T) + \frac{\partial}{\partial x_i}(U_i \rho T) = \frac{\partial}{\partial x_i}\left[\left(\frac{\mu_t}{\sigma_t} + \frac{\mu_l}{\sigma_l}\right)\frac{\partial T}{\partial x_i}\right] + \Phi \quad (3)$$

2.1.1 Turbulence equations. The turbulent viscosity, μ_t, appearing in equations (2) and (3) can be defined using the two-equation k-ε model of turbulence. According to this model (Rodi, 1984),

$$\mu_t = C_\mu \rho k^2/\varepsilon \quad (4)$$

where C_μ is an empirical constant and k is the *Turbulence kinetic energy* which is given by (Rodi, 1984)

$$\frac{\partial}{\partial t}(\rho\varepsilon) + \frac{\partial}{\partial x_i}(\rho U_i k) = \frac{\partial}{\partial x_i}\left[\left(\frac{\mu_t}{\sigma_k} + \mu\right)\frac{\partial k}{\partial x_i}\right] + G - \rho\varepsilon \quad (5)$$

similarly ε is the *Energy dissipation* given by

$$\frac{\partial}{\partial t}(\rho\varepsilon) + \frac{\partial}{\partial x_i}(\rho U_i \varepsilon) = \frac{\partial}{\partial x_i}\left[\left(\frac{\mu_t}{\sigma_\varepsilon} + \mu\right)\frac{\partial \varepsilon}{\partial x_i}\right] + \frac{\varepsilon}{k}(C_1 G - C_2 \rho\varepsilon) \quad (6)$$

where G is the rate of generation of turbulent kinetic energy while $\rho\varepsilon$ is its destruction rate. G is given by:

$$G = \mu_t\left[\left(\frac{\partial U_i}{\partial x_j} + \frac{\partial U_j}{\partial x_i}\right)\frac{\partial U_i}{\partial x_j}\right] \quad (7)$$

The model contains six empirical constants which are assigned the following values:

(1) $C_\mu = 0.09$

(2) $C_1 = 1.44$

(3) $C_2 = 1.92$

(4) $\sigma_k = 100$

(5) $\sigma_\varepsilon = 1.00$

In general, the k-ε model is valid in regions where the flow is entirely turbulent. However, close to the solid walls viscous effects become dominant and this model may not predict the flow properties correctly (Craft *et al.*, 1993). Consequently, corrections in the k-ε model may become necessary.

2.1.2 Low-Reynolds no. k-ε correction. The Lam-Bremhorst low-Reynolds number extension to the k-ε model employs a transport equation for the total dissipation rate (Bradshaw *et al.*, 1981). It differs from the standard high-Reynolds number model due to the empirical coefficients C_μ, C_1 and C_2,which are multiplied respectively by the functions:

$$f_\mu = (1 - e^{-0.0165\,\mathrm{Re}_l})^2 \left(1 + \frac{20.5}{\mathrm{Re}_t}\right)$$

$$f_1 = 1 + \left(\frac{0.05}{f_\mu}\right)^3$$

$$f_2 = 1 - e^{-\mathrm{Re}_t^2}$$

where $\mathrm{Re}_l = (z_n\sqrt{k}/\nu_l)$ and $\mathrm{Re}_t = (k^2/\varepsilon\nu_l)$; and z_n is the distance to the nearest wall. The functions f_μ, f_1 and f_2 multiplying the three constants tend to be unity for high-turbulence Reynolds numbers (Re_l and Re_t), i.e. the model tends to become a standard k-ε model (Versteeg and Malalasekera, 1995).

2.2 Heat conduction equation

For the laser heated solid plate, the heat conduction in a stationary medium is concerned with circumstances in which the temperature T may vary with time t. Therefore, the equation yields a modified form of equation (3) with an addition of a laser heat source term. Thus:

$$\frac{\partial}{\partial t}(c_p\rho T) = \frac{\partial}{\partial x_i}\left[K\frac{\partial T}{\partial x_i}\right] + S \tag{8}$$

It should be noted that S is the unsteady spatially varying mathematical representation of the laser output power intensity distribution and is considered as Gaussian with $\frac{1}{e}$ points equal to 0.375 mm i.e. the radius of the laser heated spot from the center of the beam. Thus:

$$S = \frac{I_0}{\sqrt{2\pi b}}\exp\left(-\frac{r^2}{b^2}\right)\delta\ \exp(-\delta z)H(t - \tau) \tag{9}$$

where $(I_0/\sqrt{2\pi b})\exp(-r^2/b^2)$ is the intensity distribution across the surface, $\exp(-\delta z)$ is the absorption function and, H is the Heaviside function which is used to define the pulse length. Step input laser pulse is taken into account for the simplicity with a pulse length τ is 1.08 ms.

2.3 Boundary conditions

2.3.1 Gas side. With reference to Figure (1), four boundary conditions need to be considered, including: *impinging gas inlet, unbounded air outlet, symmetry axis and the solid wall.* These are given as follows:

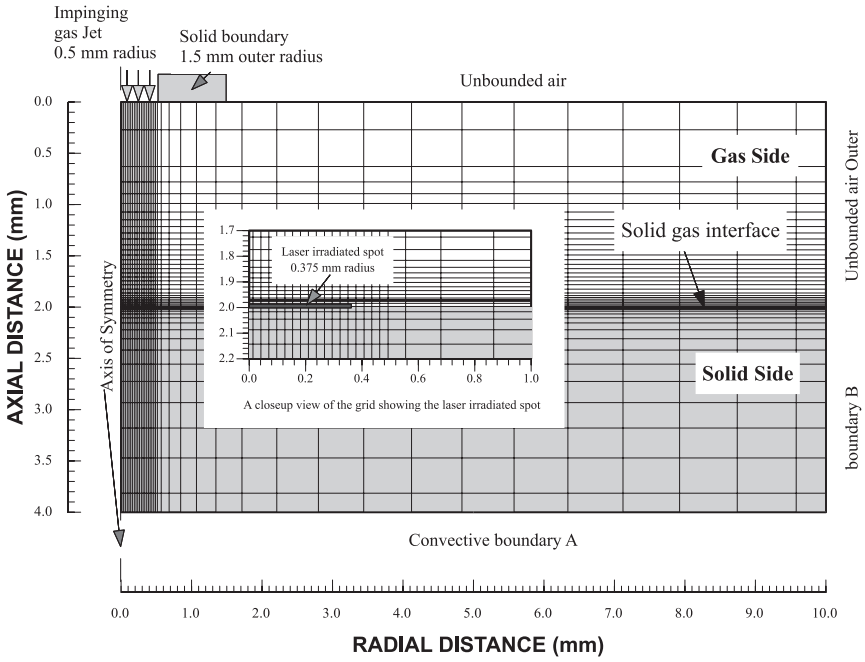

Figure 1.
The solution domain with the computational grid

Inlet conditions: The velocity profile at the nozzle exit is affected by the nozzle design such as the length-to-diameter ratio, nozzle shape, and the presence or absence of a transition section upstream of the nozzle (Amano and Brandt, 1984). In the present study, a uniform velocity profile is considered with a constant ambient temperature.

$$W = W_{jet}(1, 10, 100 \text{ and } 300\,\text{m/s}) \quad \& \quad T = T_{jet} \ (300\,\text{K}) \tag{10}$$

Values of k and ε are not known at the inlet, but some reasonable assumptions can be made. The kinetic energy of turbulence is estimated according to some fraction of the square of the average inlet velocity:

$$k = \lambda W_{jet}^2 \tag{11}$$

where λ is the turbulence intensity. The dissipation is calculated according to the equation

$$\varepsilon = C_\mu \frac{k^{\frac{3}{2}}}{\beta D} \tag{12}$$

where D is the inlet diameter and β is the length scale constant. The values $\lambda = 0.03$ and $\beta = 0.005$ are commonly used (Elkaim *et al.*, 1992).

Outlet: It is considered that the flow extends over a sufficiently long domain so that it is fully developed at the exit section. Thus for any variable ϕ the condition is

$$\frac{\partial(r\phi)}{\partial r} = 0; \qquad \frac{\partial \phi}{\partial z} = 0 \tag{13}$$

in the r and z outlet directions respectively.

Symmetry axis: Here the radial derivatives for all variables are set to zero, i.e.:

$$\frac{\partial \phi}{\partial r} = 0 \tag{14}$$

except the radial velocity which is set to zero, i.e.:

$$V = 0$$

Solid walls: At the wall the following laminar boundary conditions are set for the mean-flow variables

$$U_i = 0; \quad k = 0 \text{ and } \quad \frac{d\varepsilon}{dz} = 0$$

Since the low-Reynolds number extension does not employ wall functions, and the flow field needs to be meshed into the laminar sublayer and down to the wall, the computer storage and run-time requirements for this approach are much greater than those of the wall-function approach. In general the grid employed normal to the main flow direction needs to be distributed so as to give a high concentration of grid cells near the wall, with the wall-adjacent node positioned at $z^+ = (\rho z u^*/\mu) = 1.0$.

2.3.2 Solid side. Convection boundary: Convection with a constant coefficient for still air ($h = 5\ W/m^2$) is considered at the $z = z_{\max}$(2 mm) boundary for the plate (boundary A in Figure (1).

Constant temperature boundary: In the radial direction far away ($\sim$20 times the irradiated spot radius) from the laser source constant temperature $T = T_{\text{amb}}$(300 K) is defined (boundary B in Figure (1)). It should be noted that the constant temperature boundary condition is set at different locations in the radial directions and no significant effect of $T =$ constant was observed on the temperature and flow field in the stagnation region for distance of $\sim$20 times the irradiated spot radius.

2.3.3 Solid fluid interface. The coupling of conduction within the solid and convection within the fluid, termed conjugation, is required for the present analysis at the solid fluid interface. The appropriate boundary conditions are

continuity of heat flux and temperature and are termed boundary conditions of the fourth kind. i.e.:

$$T_{w_{solid}} = T_{w_{gas}}$$

$$K_{w_{solid}} \frac{\partial T_{w_{solid}}}{\partial z} = K_{w_{gas}} \frac{\partial T_{w_{gas}}}{\partial z}$$

No radiation losses from the solid surface is assumed.

2.4 Initial conditions

The initial conditions imposed before the initiation of laser heating, are those for the steady state stagnation heating by an impinging gas jet. The initial condition for temperature distribution is shown in Figure (2) as an example.

2.5 Variable properties

The density of air was considered to vary according to the ideal gas law depending on the local pressure and temperature; while the specific heat capacity and thermal conductivity for both air and chromium steel were considered to be a function of temperature only. The dependence of properties on temperature and pressure are given in Incropera and Dewitt (1985).

2.6 General form of the differential equations

The set of partial differential conservation equations governing the flow examined herein are compactly represented by the following non-linear elliptic partial differential equation and the accompanying Table I, which lists the dependent variables and the associated definitions of Γ_ϕ and S_ϕ.

$$\frac{\partial}{\partial t}(\rho\phi_j) + \frac{\partial}{\partial x_i}\left(\rho U_i \phi_j - \Gamma_\phi \frac{\partial \phi_j}{\partial x_i}\right) = S_{\phi_j} \tag{15}$$

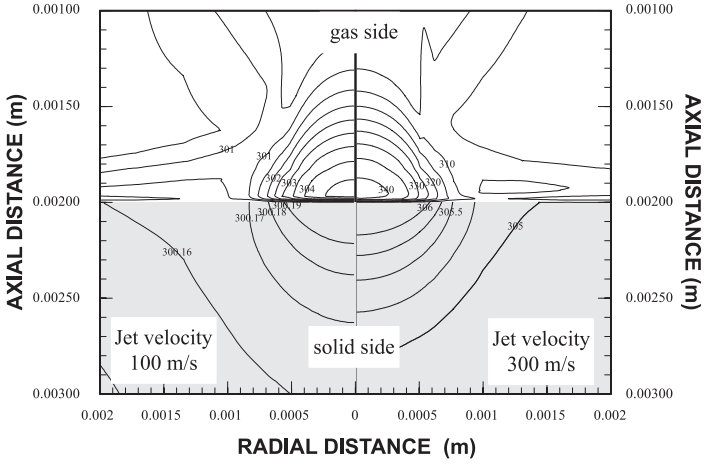

Figure 2.
Temperature contours for stagnation heating used as initial condition before the onset of laser heating

3. The numerical procedure

3.1 The control volume approach

From the differential equations governing the relevant variables, such as velocity, pressure, temperature, etc. algebraic equations are derived for the grid-point values of the variables. The calculation domain is divided into subdomains or control volumes, in this case, there is one control volume around a grid point. Each differential equation is integrated over the control volume to yield the corresponding discretization equation.

The discretization procedure is given in Versteeg and Malalasekera (1995). However, using a hybrid scheme (Patankar, 1980) the finite difference equation expressing ϕ_p, the value of ϕ at location p, in terms of the values at the nearest neighboring nodes in space and time is:

$$(a_p - S_p)\phi_p = a_n\phi_n + a_s\phi_s + a_e\phi_e + a_w\phi_w + a_l\phi_l + a_h\phi_h + a_p^o\phi_p^o + S_0 \quad (16)$$

where $a_p = \Sigma_n a_n$, $a_p^o = \rho_p^o \Delta\forall/\Delta t$ and S_o, S_p are deduced from the S_ϕ of Table I. Equations of this, kind are written for each of the variables p, V, W, k, ε, and T at every computational cell.

3.2 Calculation procedure

If the pressure field which appears as a major part of the source term for the momentum equations is known, then equation 16, written for velocities at each grid node, yields a closed set of algebraic equations, but the resulting velocity field may not satisfy the continuity relation. This problem of determining the pressure and satisfying continuity maybe overcome by adjusting the pressure field so as to satisfy continuity. A staggered grid arrangement is used in which the velocities are stored at a location midway between the grid points i.e. on the control volume faces. All other variables including pressure are calculated at the grid points. This arrangement gives a convenient way of handling the pressure linkages through the continuity equation and is known as the

Table I.
Conservation equations corresponding to equation 15; $S = I_0/\sqrt{2\pi b}\ \delta\exp(-r^2/b^2)\exp(-\delta z)$ $H(t-\tau)$ is the external source term for the solid side only and $S = 0$ for the gas side. For details of the momentum source terms $S_{Mr,z}$, refer to Versteeg and MaJalasekera (1995)

Conservation of	ϕ	Γ_ϕ	S_ϕ
Mass	1	0	0
r momentum	V	μ_e	$-\frac{\partial p}{\partial r} + S_{Mr}$
z momentum		μ_e	$-\frac{\partial p}{\partial z} + S_{Mz}$
Turbulent K E	k	μ_e/σ_k	$G - \rho\varepsilon$
Dissipation rate	ε	μ_e/σ_ε	$\frac{\varepsilon}{k}(C_1 G - C_2\rho\varepsilon)$
Temperature	T	μ_e/σ	$\Phi + S$

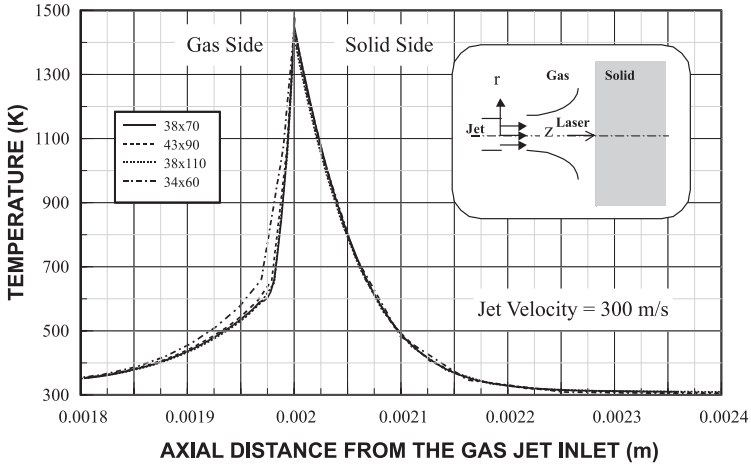

Figure 3.
The results of grid independence tests (at gas jet inlet to control volume $z = 0$)

SIMPLE (*SemiImplicit Method for Pressure-Linked Equations*) algorithm. The details of this algorithm are given in Versteeg and Malalasekera (1995).

3.3 Computation

The computer program used for the present simulation can handle a non-uniform grid spacing. In each direction fine grid spacing near the gas jet impinging point and the laser heated spot is allocated while gradually increased spacing for locations away from the center of the heated spot is considered. The non-uniform grid is designed such that the circular jet and the circular laser heated spot in the wall are represented by twenty polar cells, which have total areas equal to the area of the jet. Elsewhere the grid spacing is adjusted to maintain a constant ratio of any of two adjacent spacings. The grid generated in the present study is shown in Figure (1). The number of grid planes used normal to the y and z directions are 38 and 70, respectively, thus making a total of 2660 grid points. The grid independence tests results are shown in Figure (3). It may be observed that for 43×90 grid points the temperature resulted is almost in agreement with the results of 38×70 grid points, i.e. the peak temperature difference is less than 1 per cent.

Six variables are computed at all grid points; these are: the two velocity components, the local pressure, the two turbulence quantities and the temperature.

4. Validation of predictions

To validate the temperature profiles predicted in the solid side due to different gas jet velocities, comparison is made with the analytical solution of one-dimensional transient heat conduction equation for a semi-infinite solid allowing for convective losses from the solid surface (Blackwell 1990). The

analytical solution obtained by Blackwell (1990) is given in appendix I. The closed form solution for steel gives results only within the nanoseconds time domain, therefore, the numerical simulations are repeated within this time domain. This also justifies the comparsion of a semi-infinite solution with the present finite thickness ($z_{max} = 2$ mm) case, since the heat affected depth is (0.2μm as seen in Figure 4) which is $10^{-4} z_{max}$. Consequently, a power intensity of 4.87×10^{11} W/m^2 is introduced to achieve the temperature range similar to that obtained from the original simulation, in which a millisecond pulse is considered. In addition the closed form solution is obtained for constant properties, therefore, the simulations for validation purpose are also carried out for constant properties for consistency. The heat transfer coefficient required for the analytical solutions are obtained from the numerical predictions.

Figure (4) shows the predictions and analytical solutions for different gas jet velocities and three heating times. It is evident that the predictions and the results obtained from the analytical solution are in good agreement. However, some small discrepancies occur between both results, which may be due to one or all of the following reasons: i) the analytical solution assumes one-dimensional heating, and ii) the heat transfer coefficient is assumed to be constant in the analytical solution whereas it is time dependent in the simulation. Moreover, as the distance from the surface increases the temperature predicted at high gas jet velocity (300 m/s) attains a slightly higher value than that obtained from the analytical solution. This is due to the initial conditions imposed which involves stagnation heating by the impinging gas before the laser heating is started. These initial conditions for temperature are shown in Figure (2).

Figure (5) shows the normalized radial velocity profiles predicted and obtained from measurement (Ashforth-Frost and Jambunathan 1996). The predictions and experimental results agree well at the jet axis, close to the solid surface. As the radial distance increases, discrepancies occur between both results. In this case, the normalized velocity predicted reaches its maximum, but as the jet develops further in the radial direction the predicted profiles improve progressively. The discrepancies between the predicted and experimental results occur due to i) the developing radial flow in an axisymmetric geometry is moving into continually enlarging area; in this case, the flow characteristics in axisymmetric flow differs from those in a two-dimensional flow (Ashforth-Frost and Jambunathan, 1996), and ii) the model introduced does not account propertly for the sensitivity of the impinging jet to streamline curvature effects due to lateral divergence of the flow as indicated in the previous study (Craft *et al.*, 1993). In addition, the predictions agree well with the experimental findings as the axial distance from the solid surface increases.

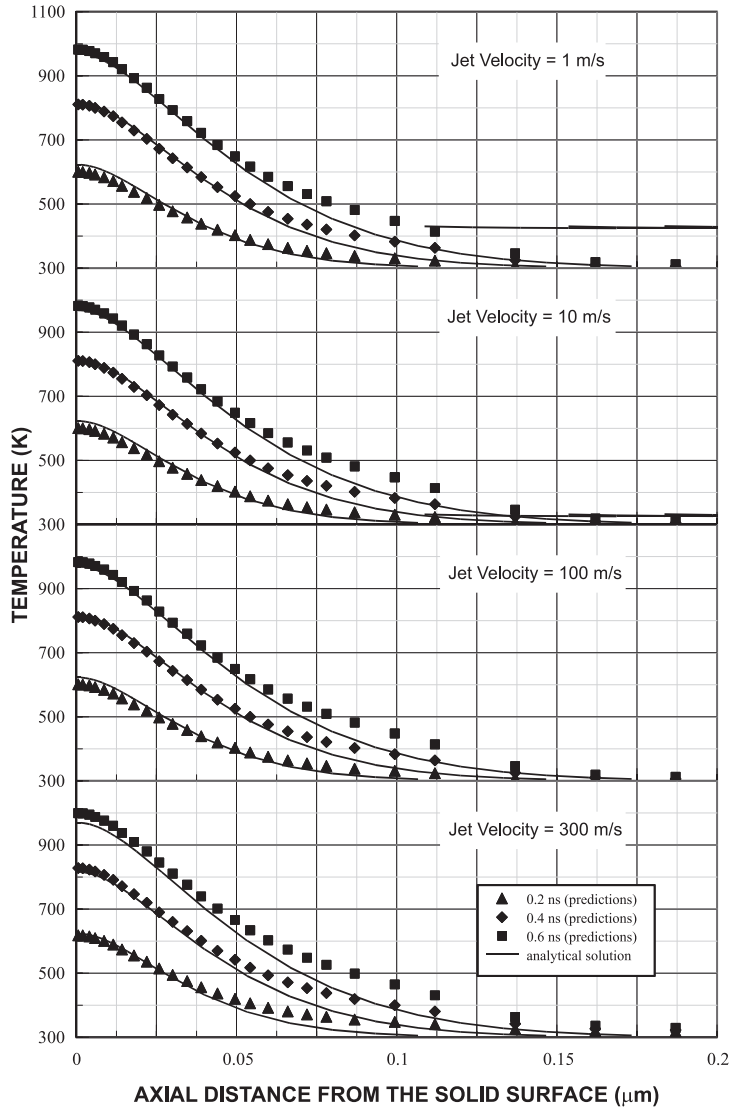

Source: Blackwell (1990)

Figure 4. Temperature distribution in the solid obtained from the present simulation and the analytical solution by Blackwell (1990) with nano second pulse and for four gas jet volocities

5. Discussion

The simulation of two-dimensional axisymmetric single pulse laser heating of steel allowing the assisting gas jet effect is carried out for a variable properties case. The standard k-ε high Reynolds number model, 2-layer k-ε model, k-ε low Reynolds number model and two Reynolds Stress Turbulence Models (RSTM-I

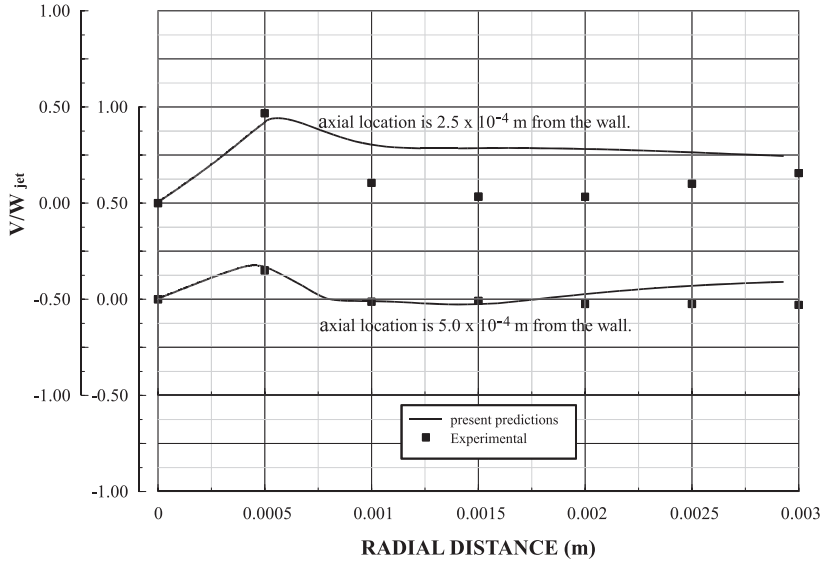

Source: Experimental is Ashforth-Frost and Jambunathan (1996)

Figure 5.
Normalized radial velocity versus radial distance; gas jet velocity is 300 m/s. Experimental is Ashforth-Frost and Jambunathan (1996)

and RSTM-2) are tested for a stagnation point flow with a constant heat flux source at the wall. RSTM-1 is the Reynolds Stress Turbulence Model in which the turbulent fluxes of energy is represented by a generalized gradient-diffusion model, i.e. these turbulent fluxes are assumed to be an algebraic function of the Reynold stresses. In addition, in the second Reynolds Stress Turbulence Model (RSTM-2) the full flux transport model is used (Launder, 1989b). The resulting Nusselt number variation due to different turbulence models and the previous experimental findings (Jambunathan *et al.*, 1992) is shown in Figure (6). The conditions for the previous study is given in appendix II. The Nusselt number does not vary considerably across the heated spot. Moreover, the standard k-ε model predicts the highest Nusselt number. This may occur because this model predicts excessive kinetic energy loss in the surface vicinity (Craft *et al.*, 1993). When comparing the Nusselt number variation across the heated spot due to the various turbulence models employed, it can be observed that low Reynolds number k-ε model gives closer results to the previous study (Jambunathan *et al.*, 1992). Therefore, this model is considered at present to account for the turbulence.

Figure (7) shows the variation of temperature with heat transfer coefficient in steel at different depths as obtained from the analytical solution (Blackwell 1990). The surface temperature remains almost constant for the heat transfer coefficient in the range $h \leq 10^7$ W/m^{2}K. This indicates that gas jet velocities which result in heat transfer coefficient less than 10^7 W/m^{2}K has no effect on the resulting surface and inside temperature distribution. When examining

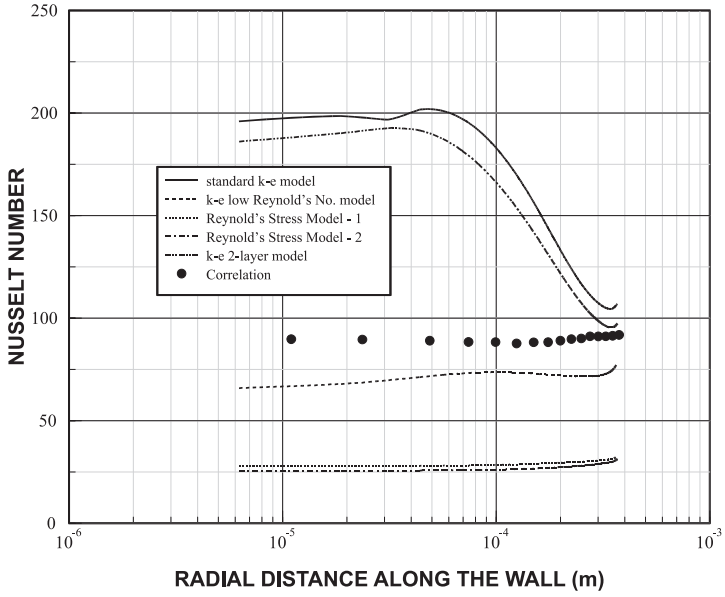

Source: Correlation by Jambunathan *et al*. (1996)

Figure 6.
Nusselt number distribution obtained from various turbulence models with variable properties. Correlation by Jambunathan *et al.* (1996)

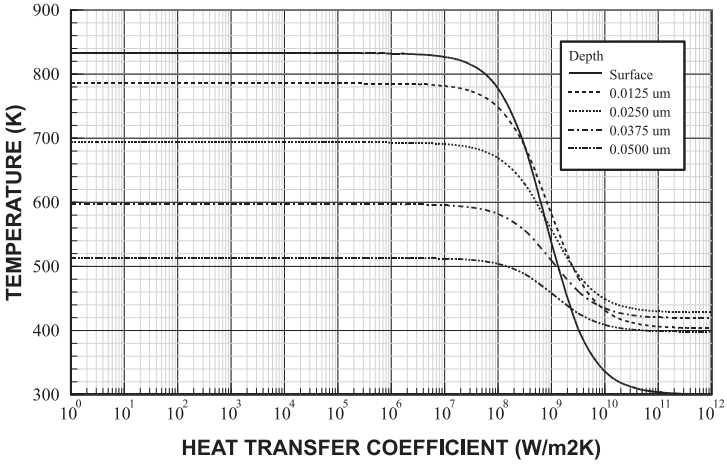

Source: Blackwell (1990)

Figure 7.
Variation of temperature with heat transfer coefficient at various depths for the analytical solution by Blackwell (1990)

Figure (8a) in which the heat transfer coefficients obtained at the surface is shown, it is evident that they are of the order of 10^4 W/m^{2}K, which is considerably small. Therefore, the internal energy gain of the substrate and the conduction due to laser heating dominate the energy losses from the surface due to convection as evident from Figure (8b), in which the ratio of absorbed energy to convection energy is shown. The ratio is in the order of 10^{-3}, i.e. the convection losses from the surface is negligibaly small. In this case, the convective losses from the surface are not high enough to influence the temperature profiles for the range of gas jet velocities considered. Moreover, the ratio of energy convected from the surface due to impinging gas jet to energy absorbed by the solid (E_{conv}/E_{in}) behaves similar to the heat transfer coefficient

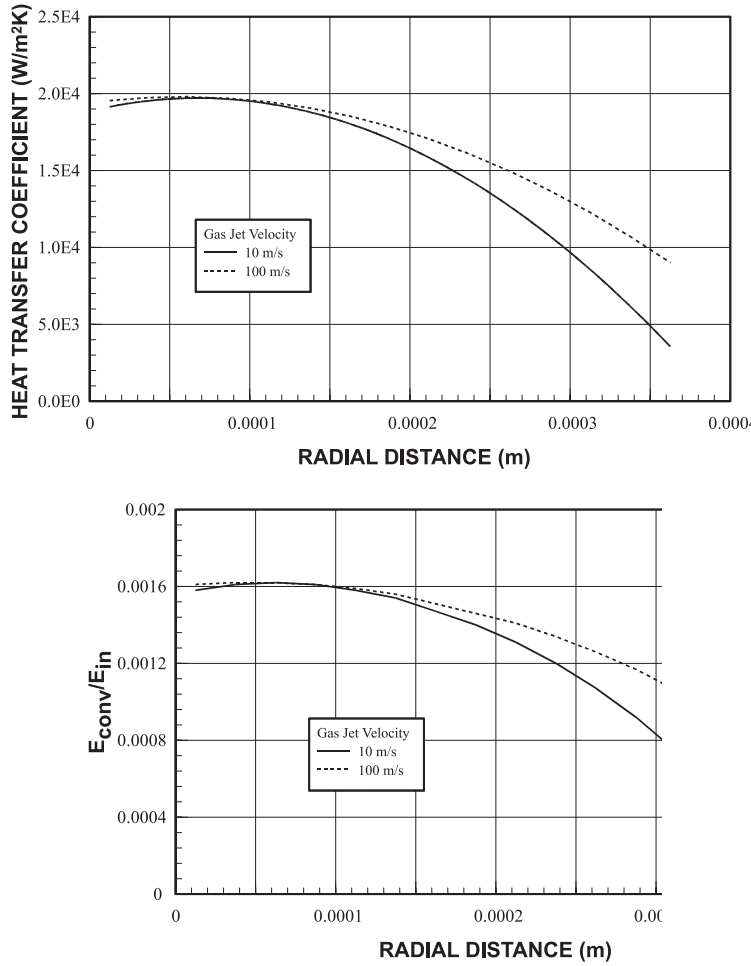

Figure 8.
(a) Variation of heat transfer coefficient with radial distance along the wall for two typical gas jet velocities (time = 1.08 ms i.e. end of heating). (b) Ratio of energy convected from surface to energy input to the solid due to laser irradiation with radial distance along the wall for two typical gas jet velocities (time = 1.08 ms i.e. end of heating)

along the radial distance. This is because the heat transfer coefficient, the temperature, and the energy absorbed by the substrate decrease as the distance along the radial direction increases from the center of the heated spot.

Figure (9) shows the temperature distribution along the axial distance for heating and cooling times, and four jet velocities at a radial location of 0.0125 mm and 0.3625 mm from the irradiated spot center. The gas jet velocity has no significant effect on the temperature profiles inside the solid. However, the gas side temperature in the surface vicinity attains sharp temperature gradient as the gas jet velocity increases. This occurs because the pressure differential in the radial direction increases with increasing gas jet velocity which in turn accelerates the radial flow and enhances the mixing of the heated fluid with the cool gas jet. This, then, results in a sharp gradient of the gas side temperature in the surface vicinity. The effect of the laser intensity distribution (spatial distribution) on the resulting temperature profiles is evident in the heating cycle. In this case, the temperature gradients in the solid side associated with two radial locations differ. The effect of initial condition due to stagnation heating on the temperature profiles in the solid side is more pronounced at 300 m/s gas jet velocity, in which case the temperature profiles in the solid side is slightly higher than those corresponding to other gas jet velocities.

Figure (10) shows the temporal response of temperature for different gas jet velocities and different locations in solid and gas sides. The difference between the solid and gas side temperature increases as the gas jet velocity increases. In this case, the rate of radial flow enhances as the gas jet velocity increases, reducing the thermal boundary layer thickness and increasing the temperature gradient in the gas side. As the distance from the surface, inside the solid substance increases, the temporal variation of the temperature becomes almost identical for all gas jet velocities. Alternatively, as the distance from the surface towards the gas side increases, the effect of heat diffusion is more pronounced at low gas jet velocities than at high gas jet velocities. In this case, the fluid heated sweeps away at a fast rate at high gas jet velocity which in turn reduces the temperature rise in this region. The stagnation point heating is evident at 300 m/s gas jet velocity (Figure (10). The temperature rises slightly higher at 300 m/s than that corresponding to a 100 m/s gas jet velocity, and also the temperature decay rate in the gas side close to solid surface increases in the cooling cycle as the gas jet velocity increases. The rate of temperature rise in both solid and gas sides becomes the same for all gas jet velocities as the heating time increases.

Figures (11) and (12) show the temperature contours resulting from both constant and variable properties for two gas jet velocities. The variable properties introduced for solid and gas jet have considerable effect on the resulting temperature profiles. In the case of variable properties, the temperature in the solid substrate attains lower values than that corresponding to constant properties. This may occur due to one or all of the following facts:

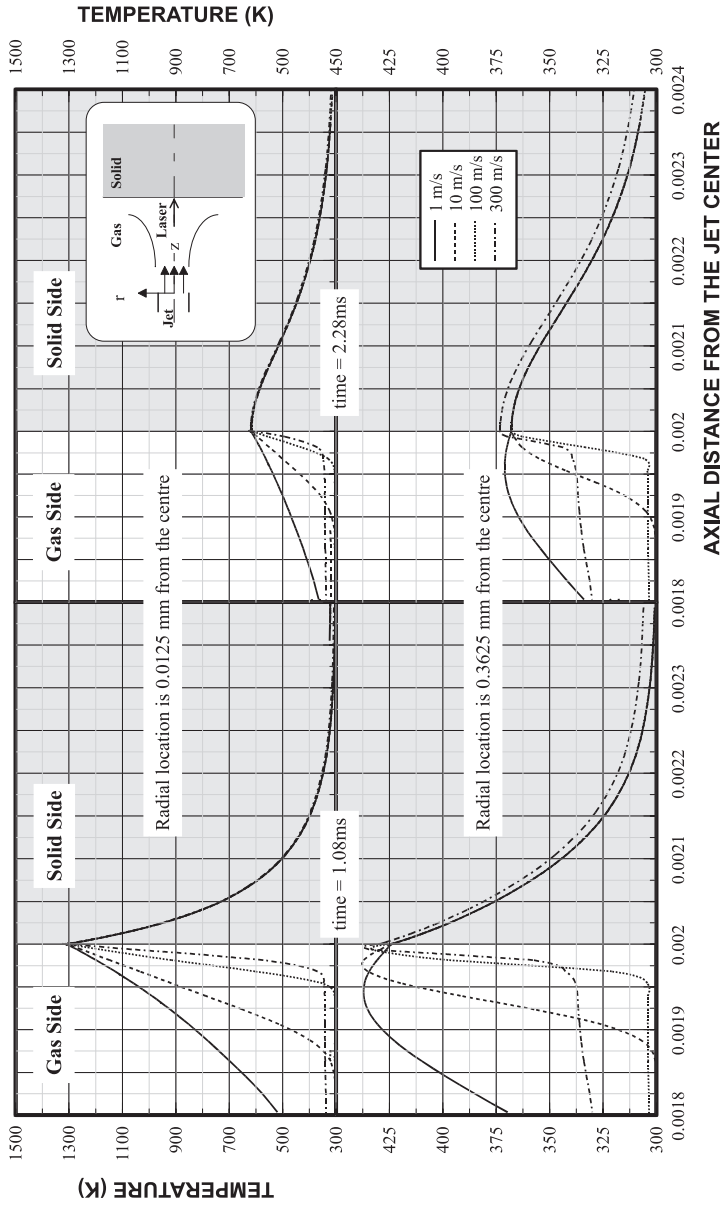

Figure 9.
Temperature profiles in the axial direction for different gas jet velocities

(1) The specific heat increases with increasing temperature, which reduces the temperature rise in the solid. Also, the thermal conductivity of the solid substrate reduces as the temperature increases, which in turn results in less heat being conducted into the solid.

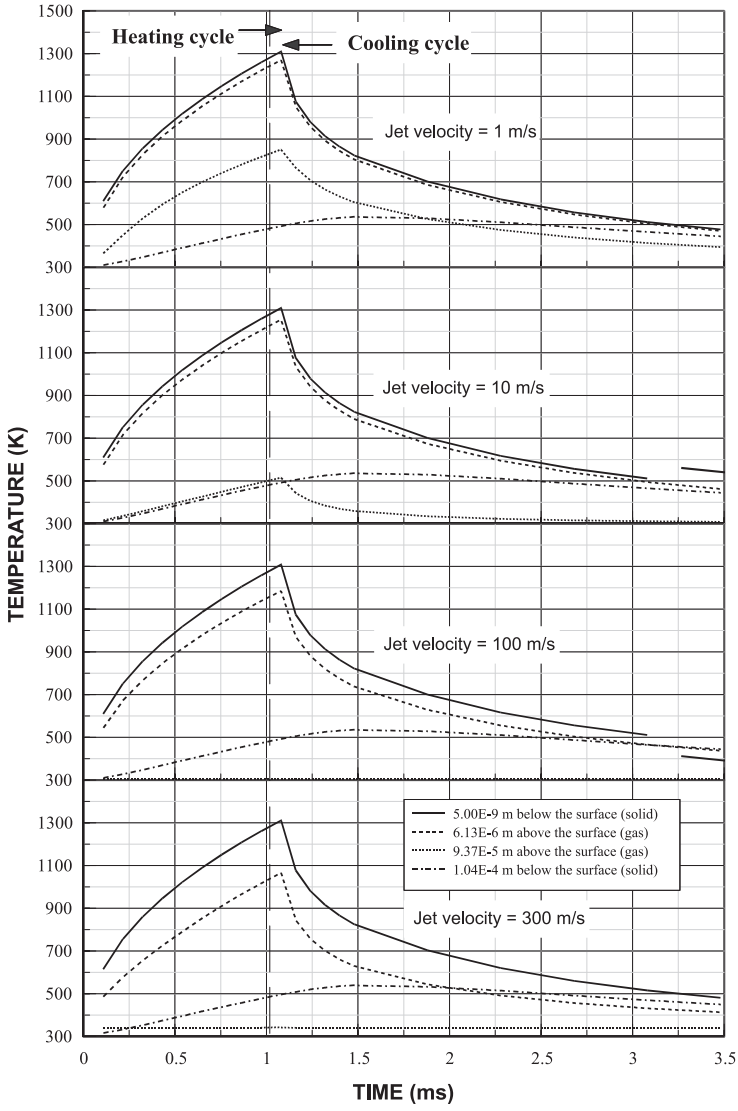

Figure 10.
Variation of temperature with time at four axial locations (two above and two below the surafce); radial location is 0.0125 mm from the centre of the jet

(2) The density of the gas reduces considerably in the surface vicinity which increases the turbulent diffusion in this region (Strahle *et al.*, 1987). Consequently, the heat diffusion is enhanced giving rise to the extension of the high temperature field in the gas jet.

The last argument becomes more pronounced in the gas side as the radial distance increases from the irradiated spot center. However, in the cooling cycle, the temperature profiles corresponding to variable properties extend

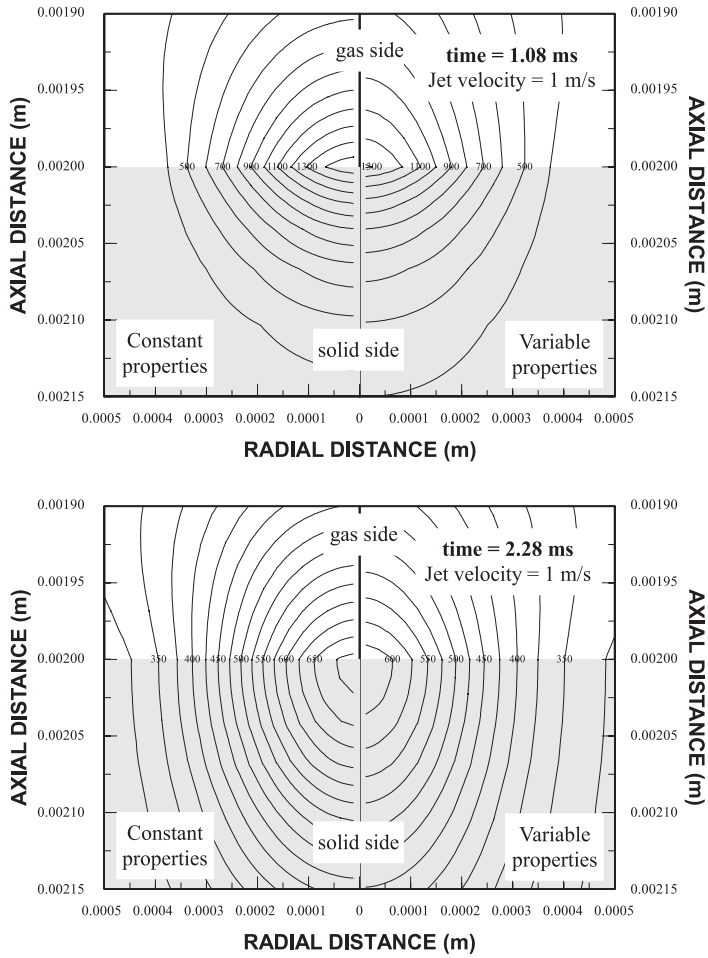

Figure 11.
Comparison of temperature contours for variable and constant properties

further in the solid substrate giving rise to high temperature attainment in the region axially away from the irradiated spot center. Alternatively, in the region close to the irradiated spot center, the temperature reaches lower values as compared to the case for constant properties.

At high gas jet velocities, the simulation results obtained from the constant properties gives high surface and inside temperatures of the solid substrate. This argument is also valid for the gas side in the surface vicinity. In this case, high gas jet velocity generates a high pressure region close to the surface, which then extends into the jet at some distance away from the surface. In addition, the density becomes low only in the region very close to the surface due to the high surface temperature, however, in the high pressure region it increases to high values and becomes almost constant. Therefore, the effect of

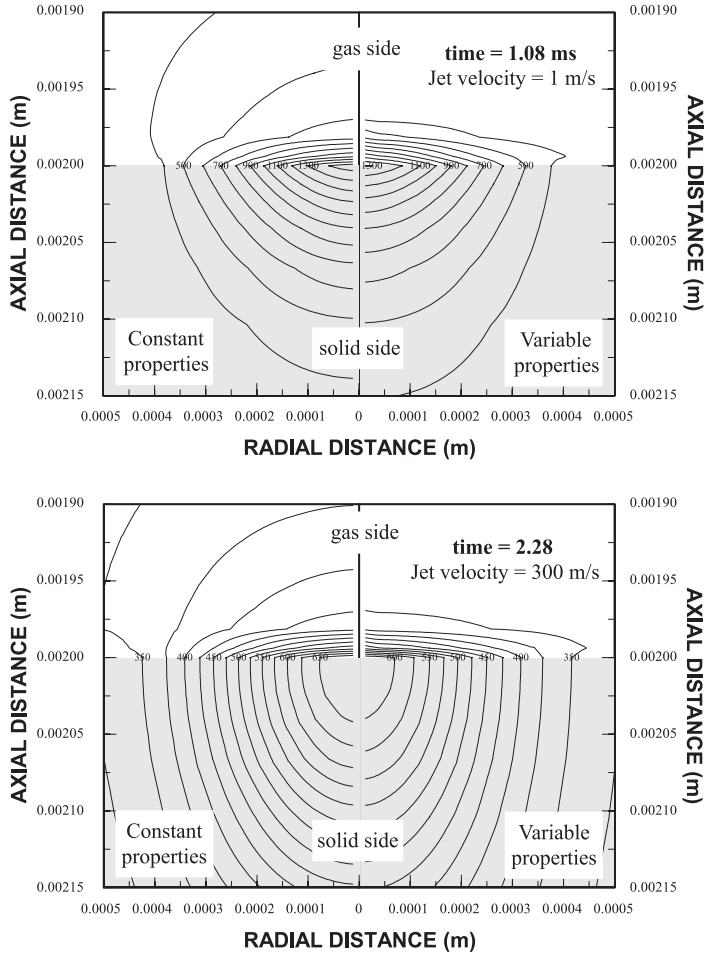

Figure 12.
Comparison of temperature contours for variable and constant properties

thermal diffusion in the gas side becomes almost similar to the constant properties case. On the other hand, attainment of low density in the surface vicinity increases the local pressure further. This then accelerates the radial flow and increases the convective cooling of the surface, i.e. the surface temperature reduces as compared to the constant properties case.

6. Conclusions

The conclusions derived from the present work is listed as follows:

(1) The temperature profiles at the irradiated spot center in the axial direction have not been influenced considerably by the gas jet velocity. As the radial distance from the irradiated spot center increases, the effect

of gas jet velocity on the temperature profiles becomes visible. This occurs at high gas jet velocity and the temperature rise due to stagnation point flow becomes important.

(2) The temperature at the surface and inside the solid increases rapidly as the heating progresses. The temperature at the irradiated spot center rises more rapidly than that occurs at the irradiated spot edge. This reverses in the cooling cycle.

(3) The gas side temperature decays rapidly in the axial direction as the gas jet velocity increases. This may occur due to the pressure differential in the radial direction, which increases as the gas jet velocity increases, which in turn accelerates the radial flow and enhances the mixing of the heated gas with the impinging gas. This is more pronounced as the radial distance from the irradiated spot center increases. The gas side temperature reduces across the irradiated spot surface as the gas jet velocity increases. In this case, convective loss increases due to enhancement of the radial flow.

(4) The variable properties introduced for solid substrate and impinging gas have significant effect on the resulting temperatures.

(5) In the cooling cycle, the temperature profiles obtained for variable properties extend further inside the solid substrate. The surface and inside temperatures become higher in the case of constant properties as compared to those obtained for variable properties.

(6) In the case of the gas side, higher temperatures are attained close to the surface for the constant properties. The low temperature attainment in the gas side for the variable properties case is, again, due to the density variation in the region close to the surface.

References

Abid, R. and Speziale, C.G. (1996), "The freestream matching condition for stagnation point turbulent flows: an alternative formulation", *Journal of Applied Mechanics*, Vol. 63, pp. 95-100.

Al-Nimr, M.A. and Masoud, S.A. (1997), "Non-equilibrium laser heating of metal films", *ASME Journal of Heat Transfer*, Vol. 119, pp. 188-90.

Amano, R.S. and Brandt, H. (1984), "Numerical study of turbulent axisymmetric jets impinging on a flat cavity and flowing into an axisymmetric cavity", *ASME J. Fluids Engineering*, Vol. 106, pp. 410-7.

Ariel, P.D. (1993), "Stagnation point flow - a free boundary value problem formulation", *International Journal of Computer Mathematics*, Vol. 49 No. 1-2, pp. 123-31.

Ashforth-Frost, S. and Jambunathan, K. (1996), "Numerical prediction of semi-confined jet impingement and comparisons with experimental data", *International Journal of Numerical Methods in Fluids*, Vol. 23, pp. 295-306.

Baukal, C.E. and Gebhart, B. (1996), "A review of semi-analytical solutions for flame impingement", *International Journal of Heat and Mass Tranfer*, Vol. 39 No. 4, pp. 2989-3002.

Blackwell, B.F. (1990), "Temperature profile in semi-infinite body with exponential source and convective boundary conditions", *ASME Journal of Heat Transfer*, Vol. 112, pp. 567-71.

Bradshaw, P., Cebeci, T. and Whitelaw, J.H. (1981), *Engineering Calculation Methods for Turbulent Flow*, chapter 3. Academic press, New York, 51 pp.

Craft, T.J., Graham, L.J.W. and Launder, B.E. (1993), "Impinging jet studies for turbulence model assessment-ii. an examination of the performance of four turbulence models", *International Journal of Heat and Mass Transfer*, Vol. 36 No. 10, pp. 2685-97.

Diniz Neto, O. and Lima, C.A.S. (1994), "Nonlinear three-dimensional temperature profiles in pulsed laser heated solids", *Journal of Physics D, Transactions of Applied Physics*, Vol. 27, pp. 1795-804.

Elkaim, D., Reggio, M. and Camarero, R. (1992), "Simulating two-dimensional turbulent flow by using the k-ε model and the vorticity-stream function formulation", *International Journal for Numerical methods in Fluids*, Vol. 14, pp. 961-80.

Incropera, F.P. and Dewitt, D.P. (1985), *Introduction to Heat Transfer*, Appendix A John Wiley & Sons, New York, pp. 667-96.

Jambunathan, K., Lai, E., Moss, M.A. and Button, B.L. (1992), "A review of heat transfer data for single circular jet impingement", *International Journal of Heat and Fluid Flow*, Vol. 13, pp. 106-15.

Kerr, O.S. and Dold, J.W. (1994), "Periodic steady vortices in a stagnation-point flow", *Journal of Fluid Mechanics*, Vol. 276, pp. 307-25.

Launder, B.E. (1989a), "Second-moment closure and its use in modelling turbulent industrial flows", *International Journal for Numerical Methods in Fluids*, Vol. 9, pp. 963-85.

Launder, B.E. (1989b), "Second-moment closure: present ... and future?", *International Journal of Heat and fluid flow*, Vol. 10 No. 4, pp. 282-300.

Loze, M. and Wright, C.D. (1997), "Temperature distributions in semi-infinite and finite thickness media as a result of absorption of laser light", *Applied Optics*, Vol. 36, pp. 494-507.

Osawa, M., Yoneyama, T. and Isskiki, Y. (1995), "Effect of laser treatment on inter-granular corrosion of austenitic stainless steel", *Corrosion Engineering*, Vol. 44 No. 3, pp. 159-65.

Patankar, S.V. (1980), *Numerical Heat Transfer*, McGraw-Hill, New York.

Qiu, T.Q. and Tien, C.L. (1994), "Femtosecond laser heating of multi-layer metals - i. analysis", *International Journal of Heat and Mass Transfer*, Vol. 37 No. 17, pp. 2789-97.

Rodi, W., (1984), *Turbulence Models and their Application in Hydraulics - A State of the Art Review*. International Association for Hydraulic Research, University of Karlsruhe, Karlsruhe, Federal Republic of Germany, 2nd edition.

Schultz, W., Becker, D., Franke, J., Kemmerling, R. and Herziger, G. (1993), "Heat conduction losses in laser cutting of metals", *Journal of Physics D, Transactions of Applied Physics*, Vol. 26, pp. 1357-63.

Shuja, S.Z. and Yilbas, B.S. (1998), "Pulsative heating of surfaces", *International Journal of Heat and Mass Transfer*, Vol. 41, pp. 3899-918.

Simon, G., Gratzke, U. and Kroos, J. (1993), "Analysis of heat conduction in deep penetration welding with a time-modulated laser pulse", *Journal of Physics D, Transactions of Applied Physics*, Vol. 26, pp. 862-9.

Strahle, W.C.K., Sigman, R. and Meyer, W.L. (1987), "Stagnation turbulent flows", *AIAA Journal*, Vol. 25 No. 8, pp. 1071-7.

Sun, Y., Weng, C., Tei-Chen, C. and Li, W. (1996), "Estimation of surface absorptivity and surface temperature in laser surface hardening process", *Japanese Journal of Applied Physics*, Vol. 35 No. 6A, pp. 3658-64.

Versteeg, H. K. and Malalasekera, W., (1995), *An Introduction to Computational Fluid Dynamics, The Finite Volume Method*. Longman Scientific and Techinical.

Yeckel, A., Strong, L. and Middleman, S. (1994), "Viscous film flow in the stagnation of the jet impinging on planar surface", *AIChE Journal*, Vol. 40, pp. 1611-7.

Yilbas, B.S. (1993), "Analytical solution for heat conduction mechanism appropriate to the laser heating process", *International Communications Heat and Mass Transfer*, Vol. 20, pp. 545-55.

Yilbas, B.S. (1997), "Laser heating process and experimental validation", *International Journal of Heat and Mass Transfer*, Vol. 40 No. 5, pp. 1131-43.

Appendix 1

The equation describing the closed form solution for the heat conduction equation in one-dimensional semi-infinite body with convective boundary conditions was obtained by Blackwell (1990). The governing conduction equation and relevant boundary conditions are given below:

The conduction equation with constant properties is:

$$\rho c_p \frac{\partial T}{\partial t} = K \frac{\partial^2 T}{\partial z^2} + S$$

for material that absorbs the laser energy internally the energy source term is:

$$S = I_0(1 - R)\delta \ \exp(-\delta z)$$

where I_0 is the laser incident intensity, R is the surface reflectivity and δ is the absorption coefficient. The initial conditions satisfy the uniform temperature i.e:

$$T(z, 0) = T_0 \tag{17}$$

and the boundary conditions at the surface and at infinite depth are

$$-K \frac{\partial T(0, t)}{\partial z} = h[T_\infty - T(0, t)] \quad \frac{\partial T(\infty, t)}{\partial z} = 0$$

The solution of the heat conduction equation is

$$T - T_0 = (T_\infty - T_0)\left[\mathrm{erfc}\left(\frac{z}{2\sqrt{\alpha t}}\right) - \exp\left(\frac{h^2}{K^2}\alpha t + \frac{hz}{K}\right)\mathrm{erfc}\left(\frac{z}{2\sqrt{\alpha t}} + \frac{h}{K}\sqrt{\alpha t}\right)\right]$$

$$+ \frac{I_0(1-R)}{\delta K}\left\{\left(1 + \frac{\delta K}{h}\right)\mathrm{erfc}\left(\frac{z}{2\sqrt{\alpha t}}\right) + \frac{1}{\frac{h}{\delta K}\left(\frac{h}{\delta K - 1}\right)}\exp\left(\frac{h^2}{K^2}\alpha t + \frac{hz}{K}\right)\right.$$

$$\times \mathrm{erfc}\left(\frac{z}{2\sqrt{\alpha t}} + \frac{h}{K}\sqrt{\alpha t}\right) - \frac{1}{2}\left(\frac{\frac{h}{\delta K} + 1}{\frac{h}{\delta K} - 1}\right)\exp(\delta^2\alpha t + \delta z)\mathrm{erfc}\left(\frac{z}{2\sqrt{\alpha t}} + \frac{h}{K}\sqrt{\alpha t}\right)$$

$$\left. - \frac{1}{2}\exp(\delta^2\alpha t + \delta z)\mathrm{erfc}\left(\frac{z}{2\sqrt{\alpha t}} + \frac{h}{K}\sqrt{\alpha t}\right) + \exp(-\delta z)[\exp(\delta^2\alpha t) - 1] - \right\}$$

Appendix 2

A correlation for the local Nusselt number was developed for a single circular jet impinging on a flat plate by Jambunathan *et al.* (1992) in the form

$$Nu = kRe^{a}$$

where

$$a = 0.82 - \frac{0.32}{\left(1 + A\left(\frac{r}{D}\right)^{k} + B\left(\frac{r}{D}\right)^{l}\right)\left(1 + C\left(\frac{z}{D}\right)^{m} + E\left(\frac{z}{D}\right)^{n}\right)}$$

with $A = -1.95, B = 2.23, C = -0.21, E = 0.21, k = 1.8, l = 2, m = 1.25$, and $n = 1.5$. for the present conditions Re = 19430 ($W_{jet} = 300$ m/S) and $z/D = 2.0$ was used. The variation of k with r/D for $z/D = 2.0$ is shown in Table A1.

r/D	0.00	0.05	0.10	0.15	0.20	0.25	0.30	0.35
K	0.490	0.490	0.465	0.500	0.513	0.524	0.531	0.531

Table AI.